

Organic nonvolatile memory devices with charge trapping multilayer graphene film

Yongsung Ji¹, Minhyeok Choe¹, Byungjin Cho¹, Sunghoon Song¹,
Jongwon Yoon¹, Heung Cho Ko¹ and Takhee Lee^{2,3}

¹ School of Materials Science and Engineering, Gwangju Institute of Science and Technology, Gwangju 500-712, Korea

² Department of Physics and Astronomy, Seoul National University, Seoul 151-742, Korea

E-mail: tlee@snu.ac.kr

Received 24 November 2011, in final form 31 January 2012

Published 24 February 2012

Online at stacks.iop.org/Nano/23/105202

Abstract

We fabricated an array-type organic nonvolatile memory device with multilayer graphene (MLG) film embedded in polyimide (PI) layers. The memory devices showed a high ON/OFF ratio (over 10^6) and a long retention time (over 10^4 s). The switching of the Al/PI/MLG/PI/Al memory devices was due to the presence of the MLG film inserted into the PI layers. The double-log current–voltage characteristics could be explained by the space-charge-limited current conduction based on a charge-trap model. A conductive atomic force microscopy found that the conduction paths in the low-resistance ON state were distributed in a highly localized area, which was associated with a carbon-rich filamentary switching mechanism.

(Some figures may appear in colour only in the online journal)

1. Introduction

Organic memory devices have been intensively researched as the next generation of information storage components due to their simple fabrication, low cost, and flexibility [1, 2]. In addition, their exceptional electrical memory performance, such as their low operation voltage and non-destructive readout, satisfy the strict requirements of emerging memory device technologies. A fast switching time (tens of nanoseconds) has been reported in organic memory devices by Yang's group [3, 4], however, most organic memory devices were operating with a slower switching speed [3–7]. Recently developed organic materials in combination with their fabrication and advanced memory architectures using stacking or flexible concepts have enabled practical memory applications [2, 6–16].

Graphene has become an important material that has been intensively researched because of its transparency, conduction properties, and solution processability [17, 18]. Various types of electronic or photonic devices using graphene electrodes have been introduced in the fields of light-emitting diodes, photovoltaic devices, touch-pad displays,

and memory devices [15, 19–22]. In particular, graphene has more flexibility and transmittance in a wavelength range broader than that of indium tin oxide (ITO) [17, 21, 23, 24]. To broaden the fields of graphene applications, new studies have been conducted in addition to the research on the use of graphene for transparent electrodes. Recently, graphene has been applied to the hole-transport layers of organic photovoltaic devices, used for active components for field-effect transistors, and used for memory devices [25–29].

In organic memory devices, active layers that function as memory layers are important for the operation of memory devices. To acquire organic materials with memory characteristics, insulating organic materials are blended with conducting nanoparticles or embedded with metallic interlayers because these methods are easier and more efficient than synthesizing new organic materials and this kind of fabrication process has also been applied to inorganic based memory devices [2, 30–36]. Recently Son *et al* reported the organic memory devices of structure of Al/PMMA/graphene/PMMA/ITO on flexible substrate using graphene film as embedded interlayer [27]. They demonstrated good memory performance even under bent conditions. To understand the memory phenomena, more

³ Author to whom any correspondence should be addressed.

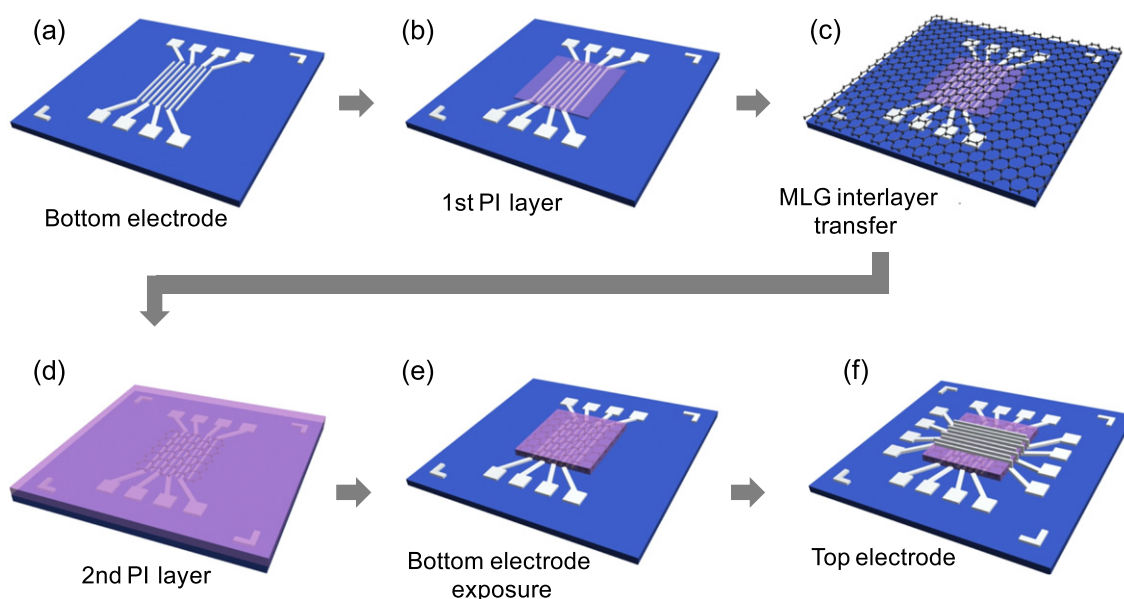


Figure 1. The fabrication of Al/PI/MLG/PI/Al memory devices.

fundamental study related to the switching effect should be conducted. Various methods such as double-log analysis of current–voltage characteristics, conductive atomic force microscopy, and energy-dispersive x-ray spectroscopy have been researched to understand the switching phenomena [27, 37–46].

In this paper, we fabricated organic memory devices in an 8×8 crossbar array with multilayer graphene film (MLG) as interlayer between insulating polyimide (PI) layers. The sheet resistance of the multilayer graphene synthesized by chemical vapor deposition (CVD) was found to be $920 \pm 70 \Omega/\square$. The organic memory devices showed write-once-read-many (WORM)-type characteristics and an excellent ON/OFF ratio of over 10^6 . The memory devices also exhibited an outstanding cell-to-cell distribution in their cumulative probability for the ON and OFF states. A retention time analysis showed stable characteristics without any significant fluctuation for over 10^4 s. The embedded MLG film trapped charges and changed the current state of the memory device in response to externally applied bias. From the conductive atomic force microscopy image, we concluded that the ON current was sustained by localized filamentary paths and the origin of the filamentary paths was from the rich carbon within PI/MLG/PI after analyzing energy-dispersive x-ray spectroscopy.

2. Experimental details

Figure 1 shows the fabrication process of organic memory devices with an MLG interlayer in PI layers. The bottom electrodes (consisting of 50 nm thick Al) were deposited by an electron beam evaporator on a Si substrate (figure 1(a)). To fabricate the insulating polymer, biphenyltetracarboxylic dianhydride p-phenylene diamine (BPDA-PPD) was prepared as the PI precursor. The BPDA-PPD was dissolved in a

solvent of *N*-methyl-2-pyrrolidone (NMP) with a weight ratio of BPDA-PPD:NMP solvent = 1:2. To enhance the film uniformity, the bottom Al electrodes were exposed to UV–ozone for 5 min. Subsequently, the PI solution was spin-coated onto the Al electrodes on the Si substrate at 2000 rpm for 40 s, followed by soft-baking on a hotplate at 60 °C for 10 min. The PI film on the Al pad was then removed and hard-baked on a hotplate at 300 °C for another 30 min (figure 1(b)). The MLG film used as the interlayer in the PI layers was synthesized in a CVD chamber on substrates deposited with 300 nm thick Ni at 900 °C under the flow of Ar gas mixed with 4% H₂, which was achieved by adding CH₄ gas. The substrate was rapidly cooled to room temperature to suppress the excessive precipitation of the carbon atoms. The graphene films were then stripped from the Ni-coated substrate using an aqueous etching solution of iron chloride (FeCl₃). The detached graphene film was transferred onto the PI/Al electrodes on the Si substrate after rinsing with de-ionized water, as shown in figure 1(c). Next, the outer region of the graphene film was removed to isolate the graphene film between the PI layers and avoid leakage paths through the Al/MLG/Al. Before spin-coating the additional PI layer onto the MLG/PI/Al on the Si substrate, the substrate was treated with UV–ozone for 5 min to improve the adhesion between the MLG film and the PI layer. Next, the second PI layer was spin-coated and soft-baked on a hotplate at 60 °C for 10 min (figure 1(d)). To expose the bottom Al pads and avoid forming bypass routes for the current, a section of the upper PI layer was removed (figure 1(e)). After the final hard-baking at 300 °C, the top Al electrodes were deposited onto the active film, as shown in figure 1(f). All electrical measurements were performed using a semiconductor characterization system (Keithley 4200-SCS) at room temperature in a N₂-filled glove box.

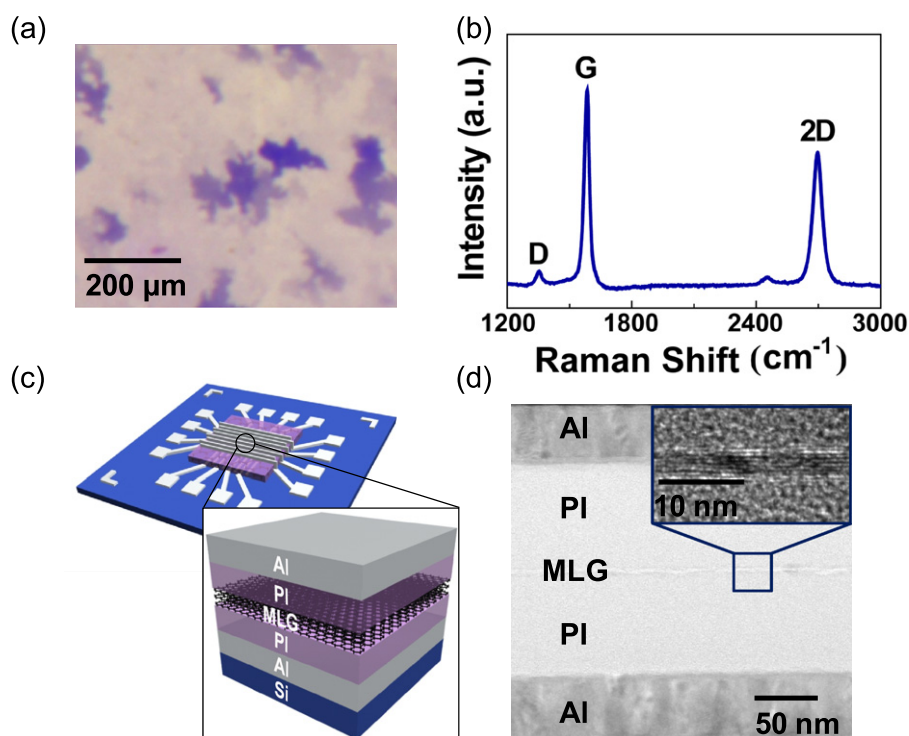


Figure 2. (a) An optical image and (b) a Raman spectrum of the MLG film. (c) A schematic of the fabricated Al/PI/MLG/PI/Al memory devices and the structure of the memory unit cell. (d) A cross-sectional TEM image of a memory device and an HRTEM image of an MLG film in the memory device (inset).

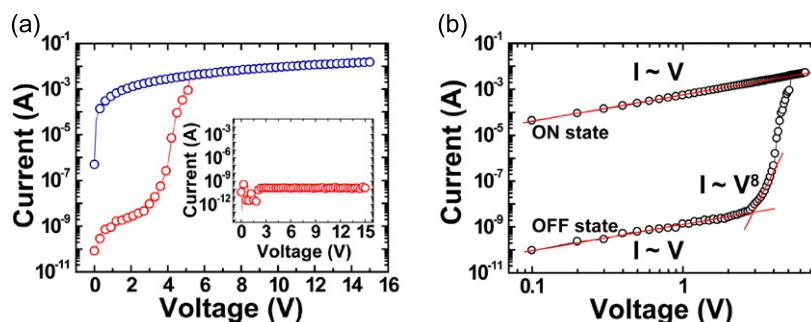


Figure 3. (a) The I - V curve of an Al/PI/MLG/PI/Al memory device and the I - V curve without an MLG film (inset). (b) A double-log I - V plot analysis of an Al/PI/MLG/PI/Al memory device.

3. Results and discussion

3.1. The characteristics of the MLG film and the structural analysis of the devices

Figure 2(a) shows an optical image of the graphene film synthesized by CVD. The light- and dark-colored regions in the optical image indicate the relatively thinner and thicker portions of the graphene film, respectively. As shown in the Raman spectra (figure 2(b)), the graphene film constituting the organic memory device was multilayered. This was validated by the result that the G-band peak at $\sim 1580\text{ cm}^{-1}$ was higher than the 2D band peak at 2700 cm^{-1} . Figure 2(c) shows a schematic of the Al/PI/MLG/PI/Al memory devices and the structure of the memory unit cell. A cross-sectional transmission electron microscopy (TEM) image of a memory

cell is shown in figure 2(d). Each layer of the active material in the memory devices could be clearly distinguished in the TEM image. The thickness of each PI layer was measured to be $\sim 80\text{ nm}$. High-resolution TEM analysis showed that the MLG film embedded within the PI layers was $\sim 3\text{ nm}$ thick (inset of figure 2(d)).

3.2. The I - V characteristics and switching mechanism of memory devices

Figure 3(a) shows the typical current-voltage (I - V) characteristics of the Al/PI/MLG/PI/Al devices. The current of the devices remained low in the low-voltage region (and in the high-resistance state (HRS)) and then gradually increased as the voltage was further increased. The current was then abruptly increased at a voltage of $\sim 3.5\text{ V}$, switching the device

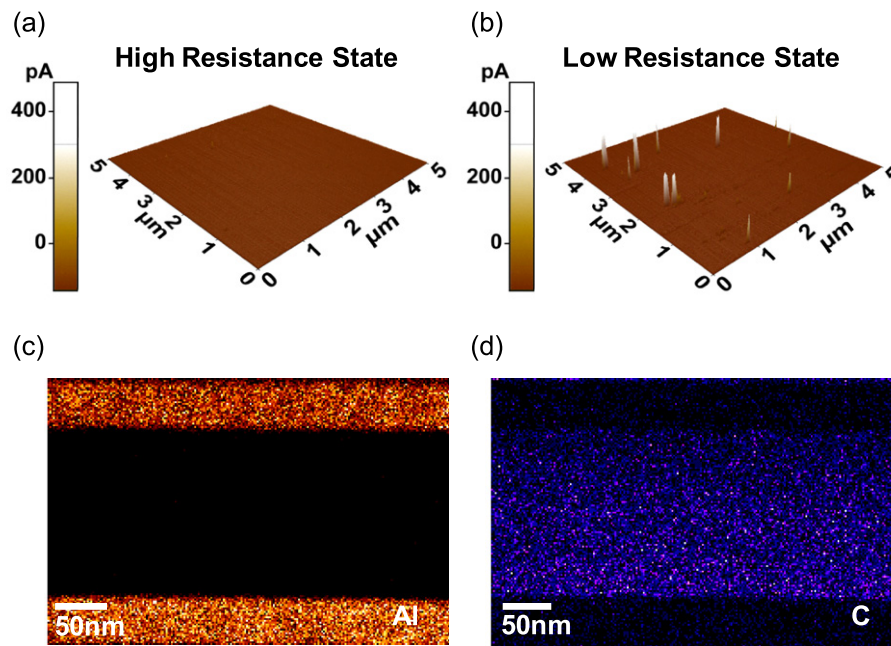


Figure 4. CAFM images of a memory device (a) at HRS and (b) at LRS. EDX analysis of (c) Al and (d) carbon element.

into a low-resistance state (LRS). The second voltage sweep from 0 to 15 V kept the device in the LRS with no current transitions and exhibited WORM-type memory characteristics with a high ON/OFF ratio of over 10^6 . The WORM-type memory device is one of the excellent data storage elements due to its permanent data saving ability without concerns on unintended data loss [40]. Moreover, WORM memory devices can be adapted in radio frequency identification devices [47]. Note that in the memory device the memory characteristics could be different according to the combination of bottom and top electrodes and interface treatment between metal electrodes and the active layer [48–52]. This may explain why WORM behavior was observed in our devices whereas switchable memory behavior was observed in other types of device structures [27]. The inset of figure 3(a) shows the I – V curve in the devices without an MLG interlayer. These devices behaved as electrically insulated devices with a very low leakage current and no current transitions. This clearly proved that the resistive memory of the Al/PI/MLG/PI/Al devices was due to the presence of the MLG interlayer. The conducting MLG films in the insulating PI layers may act as charge-trapping sites [2, 27, 53]. Charge conduction in organic devices has often been analyzed using a double-log I – V plot. Figure 3(b) shows a double-log plot analysis of the memory devices. In the low-voltage region of the OFF state, the current was linearly proportional to the applied bias and showed typical ohmic behavior. This phenomenon was due to the thermally generated free carriers at the interface between the Al and the PI layer. In the higher-voltage region (from ~ 2.6 to ~ 4 V) of the OFF state, the I – V slope of the fitting line was ~ 8 ($I \propto V^8$). This memory-switching characteristic could be explained by the space-charge-limited current (SCLC) conduction based on a trap model [2, 27, 37, 40, 41]. In this high-voltage region, a significantly large number of charge carriers were injected into the PI layer.

These charge carriers were trapped in the MLG film and participated in the current transition. The work functions of Al and MLG film are ~ 4.3 eV and ~ 4.5 eV, respectively. The PI layer was used as blocking direct contact between Al and MLG film. Once the charges are injected into the insulating film (PI) by applied bias, the charges can be trapped in the MLG layer because of the difference of potential barrier between Al and MLG and then penetrate into the second insulating layer (PI) by sufficiently applied bias. A metallic layer between the insulating layers generated a local electric field as it responded to the externally applied bias, and this local electric field affected the switching behaviors through charge rearrangement, charge hopping, or filamentary path formation [2, 27]. After this high-voltage region, the current state switched to the ON state and showed a slope of 1 ($I \propto V$), which implied that the ON current was related to the filamentary conduction [38, 39].

To support the filamentary switching characteristics of our memory devices, conductive atomic force microscopy (CAFM) was used to analyze the current distribution at each state. A conductive cantilever coated with Pt was used as a movable top electrode in the CAFM experiment. The conductive cantilever was scanned over an area of $5 \mu\text{m} \times 5 \mu\text{m}$ after making the scanned area into the HRS and LRS, where the read voltage of each state was made to be 2 V. As shown in figure 4(a), the current value of the HRS was very low throughout the entire scanned region. However, several localized current peaks were observed in the LRS state, as shown in figure 4(b). These localized current peaks suggested that the ON state was sustained by the highly localized filamentary conduction paths that formed within the PI/MLG/PI layers. Filamentary conduction paths can be generated by metallic filaments formed by metal ions injected from the metal electrodes or by carbon-rich filaments formed by the pyrolysis of the polymer with a sufficiently high electric

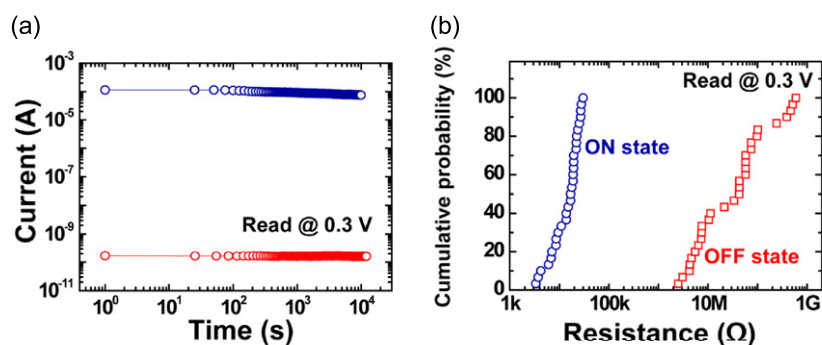


Figure 5. (a) The retention times of the memory device. (b) The cumulative probability of the memory device.

field due to the applied bias [2]. To determine the origin of the conducting paths, we analyzed the Al/PI/MLG/PI/Al layers with energy-dispersive x-ray spectroscopy (EDX). Figure 4(c) shows Al elements as yellow, indicating no Al penetration into the active layer. Figure 4(d) shows carbon elements as purple. Carbon is the major element in the active layers of PI/MLG/PI. The reason that no difference was observed between PI layers and graphene film in the active layers in figure 4(d) is because both materials (PI and graphene) are composed of carbon elements and our EDX was not able to distinguish the thin graphene film from neighboring PI layers. The important thing is that no Al filamentary metallic paths were found in the active layers, which suggests that the filamentary paths formed with the rich carbon within PI/MLG/PI layers contributed to the high current flow at the ON state. No metallic elements that were formed by the electrodes were observed within the organic layers. Thus, it can be concluded that the carbon-rich filamentary conducting paths contributed to the high current flow in the ON state.

We also investigated the memory performance and statistical uniformity of our memory devices. The retention time is an important memory parameter that is used to evaluate memory performance. As shown in figure 5(a), the memory devices showed stable characteristics over 10^4 s with no significant current fluctuations. A statistical cell-to-cell uniformity analysis was performed to confirm reliable memory operation. Figure 5(b) shows the cumulative probabilities of the ON and OFF states in 30 randomly selected operating cells. Although the OFF states were relatively broad, the ON states were well separated from the OFF states, allowing the two states to be distinguished.

4. Conclusions

In summary, we investigated organic memory devices in an 8×8 crossbar array that was fabricated with multilayer graphene film embedded in insulating polyimide layers. These memory devices showed WORM-type characteristics with an excellent ON/OFF ratio of over 10^6 , a stable retention time without fluctuations for over 10^4 s, and an outstanding cumulative probability distribution for both the ON and OFF states. The memory-switching characteristics were analyzed using a space-charge-limited conduction model (with the carriers injected from the interface between the PI and

Al electrodes), and the ON current state was sustained by localized carbon-rich filamentary current paths.

Acknowledgments

This work was supported by the National Research Laboratory program and the National Core Research Center grant of the Korean Ministry of Education, Science and Technology.

References

- [1] Sekitani T, Yokota T, Zschieschang U, Klauk H, Bauer S, Takeuchi K, Takamiya M, Sakurai T and Someya T 2009 *Science* **326** 1516
- [2] Ling Q-D, Liaw D-J, Zhu C, Chan D S-H, Kang E-T and Neoh K-G 2008 *Prog. Polym. Sci.* **33** 917
- [3] Ma L P, Liu J and Yang Y 2002 *Appl. Phys. Lett.* **80** 2997
- [4] Kwan W L, Tseng R J, Wu W, Pei Q and Yang Y 2007 *IEDM 2007* doi:10.1109/IEDM.2007.4418911
- [5] Kim T-W, Oh S-H, Lee J, Choi H, Wang G, Park J, Kim D-Y, Hwang H and Lee T 2010 *Org. Electron.* **11** 109
- [6] Cho B, Kim T-W, Song S, Ji Y, Jo M, Hwang H, Jung G-Y and Lee T 2010 *Adv. Mater.* **22** 1228
- [7] Song S, Cho B, Kim T-W, Ji Y, Jo M, Wang G, Choe M, Kahng Y H, Hwang H and Lee T 2010 *Adv. Mater.* **22** 5048
- [8] Asadi K, de Leeuw D M, de Boer B and Blom P W M 2008 *Nature Mater.* **7** 547
- [9] Kim T-W, Lee K, Oh S-H, Wang G, Kim D-Y, Jung G-Y and Lee T 2008 *Nanotechnology* **19** 405201
- [10] Kim J J, Cho B, Kim K S, Lee T and Jung G Y 2011 *Adv. Mater.* **23** 2104
- [11] Kwan W L, Tseng R J and Yang Y 2009 *Phil. Trans. R. Soc. A* **367** 4159
- [12] Kim T-W, Choi H, Oh S-H, Wang G, Kim D-Y, Hwang H and Lee T 2009 *Adv. Mater.* **21** 2497
- [13] Ji Y, Cho B, Song S, Kim T-W, Choe M, Kahng Y H and Lee T 2010 *Adv. Mater.* **22** 3071
- [14] Cho B, Song S, Ji Y and Lee T 2010 *Appl. Phys. Lett.* **97** 063305
- [15] Ji Y, Lee S, Cho B, Song S and Lee T 2011 *ACS Nano* **5** 5995
- [16] Cho B, Song S, Ji Y, Kim T-W and Lee T 2011 *Adv. Funct. Mater.* **21** 2806
- [17] Kim K S, Zhao Y, Jang H, Lee S Y, Kim J M, Kim K S, Ahn J-H, Kim P, Choi J-Y and Hong B H 2009 *Nature* **457** 706
- [18] Green A A and Hersam M C 2009 *Nano Lett.* **9** 4031
- [19] Wu J, Agrawal M, Becerril H A, Bao Z, Liu Z, Chen Y and Peumans P 2010 *ACS Nano* **4** 43

- [20] Gomez De Arco L, Zhang Y, Schlenker C W, Ryu K, Thompson M E and Zhou C 2010 *ACS Nano* **4** 2865
- [21] Bae S et al 2010 *Nature Nanotechnol.* **5** 574
- [22] Jo G et al 2010 *Nanotechnology* **21** 175201
- [23] Boehme M and Charton C 2005 *Surf. Coat. Technol.* **200** 932
- [24] Tsoukleri G, Parthenios J, Papagelis K, Jalil R, Ferrari A C, Geim A K, Novoselov K S and Galiotis C 2009 *Small* **5** 2397
- [25] Li S-S, Tu K-H, Lin C-C, Chen C-W and Chhowalla M 2010 *ACS Nano* **4** 3169
- [26] Bai J, Zhong X, Jiang S, Huang Y and Duan X 2010 *Nature Nanotechnol.* **5** 190
- [27] Son D I, Kim T W, Shim J H, Jung J H, Lee D U, Lee J M, Park W I and Choi W K 2010 *Nano Lett.* **10** 2441
- [28] Jeong H Y et al 2010 *Nano Lett.* **10** 4381
- [29] Sinitiskii A and Tour J M 2009 *ACS Nano* **3** 2760
- [30] Cho B, Kim T-W, Choe M, Wang G, Song S and Lee T 2009 *Org. Electron.* **10** 473
- [31] Baral J K, Majumdar H S, Laiho A, Jiang H, Kauppinen E I, Ras R H A, Ruokolainen J, Ikkala O and Österbacka R 2008 *Nanotechnology* **19** 035203
- [32] Chen J-R, Lin H-T, Hwang G-W, Chan Y-J and Li P-W 2009 *Nanotechnology* **20** 255706
- [33] Bozano L D, Kean B W, Deline V R, Salem J R and Scott J C 2004 *Appl. Phys. Lett.* **84** 607
- [34] Wu M-C, Lin Y-W, Jang W-Y, Lin C-H and Tseng T-Y 2011 *IEEE Electron Device Lett.* **32** 1026
- [35] Panda D, Dhar A and Ray S K 2010 *J. Appl. Phys.* **108** 104513
- [36] Panda D, Dhar A and Ray S K 2012 *IEEE Trans. Nanotechnol.* **11** 51
- [37] Kim T-W, Oh S-H, Choi H, Wang G, Hwang H, Kim D-Y and Lee T 2008 *Appl. Phys. Lett.* **92** 253308
- [38] Liu J, Yin Z, Cao X, Zhao F, Lin A, Xie L, Fan Q, Boey F, Zhang H and Huang W 2010 *ACS Nano* **4** 3987
- [39] Wang Z S, Zeng F, Yang J, Chen C, Yang Y C and Pan F 2010 *Appl. Phys. Lett.* **97** 253301
- [40] Lee T J, Chang C-W, Hahn S G, Kim K, Park S, Kim D M, Kim J, Kwon W-S, Liou G-S and Ree M 2009 *Nanotechnology* **20** 135204
- [41] Arif M, Yun M, Gangopadhyay S, Ghosh K, Fadiga L, Galbrecht F, Scherf U and Guha S 2007 *Phys. Rev. B* **75** 195202
- [42] Waser R, Dittmann R, Staikov G and Szot K 2009 *Adv. Mater.* **21** 2632
- [43] Waser R and Aono M 2007 *Nature Mater.* **6** 833
- [44] Muenstermann R, Menke T, Dittmann R and Waser R 2010 *Adv. Mater.* **22** 4819
- [45] Cho B, Yun J-M, Song S, Ji Y, Kim D-Y and Lee T 2011 *Adv. Funct. Mater.* **21** 3976
- [46] Schroeder H, Pandian R and Miao J 2011 *Phys. Status Solidi a* **208** 300
- [47] Gao J, Sidén J and Nilsson H-E 2011 *IEEE Electron Devices Lett.* **32** 1767
- [48] Verbakel F, Meskers S C J and Janssen R A J 2007 *Appl. Phys. Lett.* **91** 192103
- [49] Tsubouchi K, Ohkubo I, Kumigashira H, Oshima M, Matsumoto Y, Itaka K, Ohnishi T, Lippmaa M and Koinuma H 2007 *Adv. Mater.* **19** 1711
- [50] Mukherjee B and Pal A J 2006 *Org. Electron.* **7** 249
- [51] Sawa A 2008 *Mater. Today* **11** 28
- [52] Sawa A, Fujii T, Kawasaki M and Tokura Y 2004 *Appl. Phys. Lett.* **85** 4073
- [53] Kim T-W, Gao Y, Acton O, Yip H-L, Ma H, Chen H and Jen A K-Y 2010 *Appl. Phys. Lett.* **97** 023310